Nonlinearities shape the response patterns to oscillatory inputs in a caricature electrochemical cell model

Horacio G. Rotstein *

Federated Department of Biological Sciences
Rutgers University and New Jersey Institute of Technology, USA

January 4, 2022

Abstract

We investigate the nonlinear mechanisms of generation of preferred frequency response patterns to oscillatory inputs in a phenomenological (caricature) model that captures the type of nonlinearities present in electrochemical (EC) cells and is simple enough to begin to develop the dynamical systems tools necessary for the understanding of the relationship between the model nonlinearities and the response patterns. Previous work has shown that linearized EC models exhibit resonance (preferred frequency response to oscillatory inputs at a non-zero, resonant, input frequency) in parameter regimes where the stable equilibrium is either a node (no intrinsic oscillations) or a focus (damped oscillations). We use a combination of numerical simulations and dynamical systems tools to understand how the model nonlinearities, partially captured by the geometry of the nullclines in the phase-space diagram, shape the response patterns to oscillatory inputs away from the validity of the corresponding linearization. We develop and adapt and extended version of the classical phase-plane diagram that allows us to track the evolution of the response trajectories and their interaction with the so-called "moving nullclines" (in response to the oscillatory inputs). We use this approach to explain the mechanisms of generation of nonlinear resonant patterns, the nonlinear amplification/attenuation of these patterns by increasing input amplitudes, and the mechanisms of generation of more complex patterns of mixed-mode type where the stationary amplitude response is not uniform across cycles.

*Graduate Faculty, Behavioral Neurosciences (BNS) Program, Rutgers University. Corresponding Investigator, CONICET, Argentina.

Dynamical systems exhibit complex frequency-dependent responses to oscillatory inputs. These responses are shaped by the system's intrinsic properties and effective time scales, which depend on the dynamic process modeled. The response of linear systems to oscillatory inputs are well understood, but there is a gap in our understanding of how a system's nonlinearities affect their responses to oscillatory inputs. In this paper we address this issue in the context of a caricature mode of an electrochemical cell and develop the necessary tools to understand the underlying mechanism.

1 Introduction

The response of dynamical systems to oscillatory inputs ranges from relatively simple to very complex. The first group includes the so-called low- and band-pass filters (Fig. 1-a). In a low-pass filter the amplitude impedance profile (Z) is a decreasing function of the input frequency f (Fig. 1-a, red). Band-pass filters capture the system's ability to exhibit resonance, defined as the occurrence of a peak in Z for an intermediate input frequency f_{res} (Fig. 1-a, blue). Associated to the concept of resonance is the concept of phasonance consisting on the system's ability to exhibit a zero-phase (Φ) response to oscillatory inputs at an intermediate frequency f_{phas} (Fig. 1-b). The response is advance for $f < f_{phas}$ and delayed for $f > f_{phas}$.

The occurrence of resonance results from the interplay of external oscillatory inputs and intrinsic positive and negative feedback effects operating at different time scales [1,2]. The so-called activators provide the positive feedback effect by stimulating both their own production, via autocatalytic effects and the production of inhibitors. The latter provide the slower negative feedback effect by repressing the production of the activator.

It is sometimes believed that resonance requires the presence of intrinsic oscillations in the unforced (autonomous) system, and the role of the oscillatory perturbations is to amplify the response close to the natural (intrinsic) frequency. However, as demonstrated by us and other authors [3–8] and explained in previous work [6,7], resonance may robustly occur in the absence of intrinsic oscillations, for example, in linear two- and three-dimensional systems having a stable node. Therefore resonance is a property of the interaction between the oscillatory input and the cell's properties that uncovers a time scale (associated to the resonant frequency) that may or may not be involved in the generation of intrinsic oscillations. In the latter case we refer to it as a latent (or hidden) time scale. The presence of these latent time scales are expected to have implications for oscillatory network dynamics.

Resonance is a well understood phenomenon in linear systems. The presence of nonlinearities causes more complex responses to oscillatory inputs including nonlinear amplifications and attenuations of the response, breaking of symmetry with respect to the equilibrium value for the underlying unforced system, cycle-skipping (breaking of entrainment) and chaos [9]. There is a gap in our understanding of how the system's nonlinearities shape the response patterns to oscillatory inputs.

Several recent papers have investigated the frequency preference response properties of electrochemical (EC) systems to oscillatory inputs under various control conditions (e.g., potentiostatic, galvanostatic) [1,3,10–18]. The combined effect of the system's dynamical and physicochemical properties produces different types of response patterns including the low- and band-pass filters mentioned above. In these systems the activators are typically the electrode potentials or currents and the in-

hibitors are the surface concentrations. The dynamic mechanisms that govern these interactions to produce resonance in EC cells are not well understood.

Existing theoretical studies on resonance in EC cells have primarily focused on linear or linearized models [3, 14, 15, 18] (see also references therein) for which analytical computations can be performed using standard tools [4, 18–20], or simulations using nonlinear models [21, 22]. To our knowledge the mechanisms of generation of resonance in nonlinear models has not been investigated in detail. Moreover, the appropriate analytical tools to carry these studies are lacking.

In a recent paper [3] we have investigated the linearized resonant properties of a two-dimensional phenomenological model introduced in [23,24] to describe the dynamics of an EC-cell under potentiostatic conditions. The model consists of two dependent variables, the electrode potential (V) and the surface concentration (w). Although phenomenological, this model captures the oscillatory behavior typically observed in realistic systems [25] (e.g., limit cycle oscillations created in a Hopf bifurcation) and the existence of resonance when the stable equilibria are either nodes or foci [3]. Our method consisted on linearizing the EC model (around a stable node or focus) and tracking the dependence of the Z- and Φ-profiles (curves of Z and Φ as a function of the input frequency f) with the model parameters through the linearized parameters. Changes in a model parameter cause changes in one or more linearized parameters, which in turn cause changes in the attributes of the Z- and Φ-profiles (e.g., resonant frequency, maximal impedance). In this way we captured some aspects of the complex nonlinear nonlinear model response to oscillatory inputs, but other aspects that are inherently nonlinear (e.g., nonlinear amplifications/attenuations, the presence of non-sinusoidal responses, cycle-skipping and mixed-mode oscillatory responses) were naturally not captured by our approach.

The goal of this paper is to understand how the nonlinearities typically present in a dynamic model shape the system's response patterns to oscillatory inputs. As a case study we use phenomenological (caricature) model of ECs described in the previous paragraph that includes a rich variety of nonlinearities observed in more realistic models ranging from quasi-linear, to cubic-like to more complex ones depending on the model parameters [3]. We focus on regimes where the unforced system has a single stable equilibrium point that can be either a node (no intrinsic oscillations) or a focus (damped oscillations). For low input amplitudes the responses can be captured by the corresponding linearized system, as expected. However, for larger input amplitudes the effects of the nonlinearities become more pronounced and diverse and the linear theory fails to capture the properties of the system's response to oscillatory inputs. An additional goal of this paper is to begin to develop this theory. For simplicity, we restrict our study to additive input currents that affect only the activator equation. This approach is not realistic, and cannot be experimentally implemented in a straightforward way, but it makes our toy model simple enough to begin to develop the dynamical systems tools necessary for the understanding of the relationship between the model nonlinearities and the response patterns. As it is the case with most studies using toy models (e.g., the FitzHugh-Nagumo model used to understand neuronal dynamics [26, 27]), the response patterns that emerge from our study can then be searched for in more realistic models and the tools we develop in this paper can be used and adapted to understand these patterns.

For our analysis we use a combination of numerical simulations and dynamical systems tools. These techniques are useful for the investigation of nonlinear dynamic mechanisms by looking at the evolution of the model trajectories in the phase-space diagram (each dimension corresponding to a state variable) as time progresses. The model nonlinearities are reflected in the shapes of the zero-level sets (curves or surfaces) of the model equations. These nullclines (or nullsurfaces) capture the way in which these nonlinearities affect how trajectories evolve in the phase-space diagram. We develop

and adapt and extended version of the classical phase-plane diagram that allows us to track the evolution of the response trajectories and their interaction with the so-called "moving nullclines" (in response to the oscillatory inputs). We use this approach to explain the mechanisms of generation of nonlinear resonant patterns, the nonlinear amplification/attenuation of these patterns by increasing input amplitudes, and the mechanisms of generation of more complex patterns of mixed-mode type where the stationary amplitude response is not uniform across cycles.

The analysis presented in this paper and the tools we develop to carry out this analysis contribute to the understanding of both the nonlinear amplifications and attenuations of the EC cell responses to oscillatory inputs in the response patterns that are uniform across input cycles, but depart from the linear predictions, as well as the generation of response patterns with non-uniform properties across cycles.

2 Methods

2.1 Phenomenological EC-cell model

We consider the following phenomenological model introduced in [23] after a time rescaling (see [3] for the formulation of the original model and the time rescaling process). The conservation of charge equation is given by

$$V' = \frac{q - V}{R} - w\, p(V) + I_{in}(t) \tag{1}$$

where the "prime" sign represents differentiation with respect to the time t, V is the electrode potential, w the surface concentration, R is the ohmic resistance, q is the (baseline) applied potential, $I_{in}(t)$ is the external, time-dependent applied current, and $p(V)$ is a given function that depends on the specific details of the system. The left hand-side in eq. (1) represents the current flowing through the double layer capacitance, the first term and second terms represent the total current flowing through the system and the faradaic current due to the electrochemical reaction respectively. The surface concentration obeys the following mass balance equation

$$w' = \epsilon \left[-\frac{q - V}{R} + 1 - w + \alpha\, w\, p(V) \right], \tag{2}$$

where ϵ is the double layer capacitance (it shows in this equation because of the time rescaling mentioned above) .
The first and second terms term in the right hand-side represent diffusion and migration due to potential gradients respectively. Following [3, 23, 25] we use $\epsilon = 0.03$ and

$$p(V) = a_1\, V + a_2\, V^2 + a_3\, V^3, \tag{3}$$

where $a_1 = 1.125$, $a_2 = -0.075$ and $a_3 = 0.00125$. For these parameter values

$$p(V) = a_3\, V\, (V - 30)^2. \tag{4}$$

This is a cubic function having a maximum at $V = 10$ and a minimum at $V = 30$. The parameter α represents the strength of the nonlinearity.

For external sinusoidal inputs we use the following notation

$$I_{in}(t) = A_{in}\, sin(\Omega\, t) \qquad \text{with} \qquad \Omega = \frac{2\pi f}{T}, \tag{5}$$

We use $T = 1000$. While for EC cells under potentiostatic control the observable is the anodic current $(q - V)/R$, in this work we consider the effects of an input current and we present our results in terms of the voltage response V. We note that the addition of a current rather than a potential input does not describe either a potentiostatically or galvanostatically controlled system, thus not allowing for a direct comparison with experiments. However, the simplified approach we use in this paper provides an insight into the resonance phenomenon in electrochemical systems that can be then adapted to more realistic situations.

The time rescaling mentioned above involves moving the parameter ϵ from the left hand side of the first equation (coefficient of the derivative of V with respect to time) to the right hand side of the second equation. Technically, ϵ does not have units of time. Therefore, our rescaling is based under the hidden assumption that a constant equal to one remains as a factor in the left hand side of eq. (16) to maintain the balance of units. Note that this time rescaling also affects the time-dependent term.

2.2 Impedance and impedance-like functions

The response (after transients have worn off) of a linear system, such as linearized version of (1)-(2), receiving sinusoidal current inputs of the form (5) in the first equation is given by

$$V_{out}(t; f) = A_{out}(f)\, \sin\left(\Omega\, t - \Phi(f)\right) \tag{6}$$

where $\Phi(f)$ is the phase-shift (or phase) defined as the difference between the peaks of the input $I_{in}(t; f)$ and the output $V_{out}(t; f)$ and Ω is given by (5).

Linear systems exhibit resonance if there is a peak in the amplitude $Z(f) = |Z(f)|$ of the impedance function $\mathbf{Z}(\mathbf{f})$ given by

$$Z(f) = \frac{A_{out}(f)}{A_{in}} \tag{7}$$

at some positive (resonant) frequency f_{res} (Fig. 1-a, blue). We refer to the ability of the system to exhibit a zero-phase frequency response at a non-zero frequency as *phasonance* and to the corresponding frequency as the *phasonant* frequency f_{phas} (Fig. 1-b, blue). The response is "advanced" and "delayed" with respect to the peak of the input current for lower and higher frequency inputs respectively. Although phasonance is an important phenomenon [3], in this paper we focus on the properties of the amplitude response.

For nonlinear systems, or for linear systems with non-sinusoidal inputs, and assuming the number of input and output cicles coincide and the output amplitude is uniform across cycles for a given input (with constant amplitude), we use the following extended version of the definition of the impedance amplitude that captures the amplitude response

$$Z(f) = \frac{V_{max}(f) - V_{min}(f)}{2\, A_{in}} \tag{8}$$

where $V_{max}(f)$ and $V_{min}(f)$ are the maximum and minimum of the oscillatory voltage response $V_{out}(t, f)$ for each value of the input frequency f. For linear systems receiving sinusoidal inputs,

eqs. (8) and (7) are equivalent. Similarly to the linear case, the phase $\Phi(f)$ is computed as the distance between the peaks of the output and the input (within the same input cycle) normalized by the period.

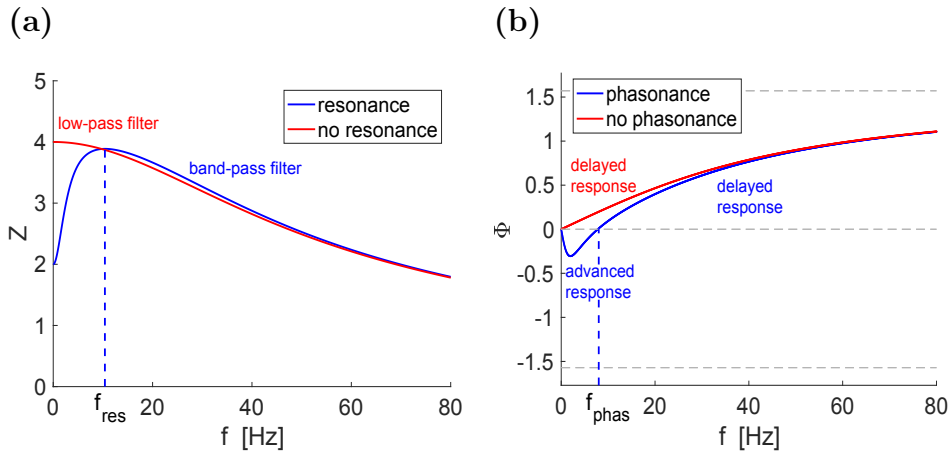

Figure 1: **Schematic diagrams of the impedance (Z-) and phase (Φ-) profiles in response to oscillatory inputs with frequencies f. (a) Z-profiles**: curves of Z as a function of f. The resonant frequency f_{res} is defined as the non-zero input frequency at which $Z(f)$ peaks. **(b) Φ-profiles**: curves of Φ as a function of f. The phasonant frequency f_{phas} is defined as the non-zero input frequency at which $\Phi(f) = 0$.

2.3 ZAP inputs and impedance

An alternative type of oscillatory input used by various authors to investigate the resonant properties of circuits is the so-called ZAP input [2, 18, 28]

$$I_{in}(t) = I_{ZAP}(t) = A_{in}\,\sin(2\,\pi\,f(t)\,t), \qquad f(t) = \frac{f_M\,t}{2\,T_M}, \tag{9}$$

that sweeps through a given range of frequencies over time with a maximum frequency f_M and a stimulus length T_M (Fig. 2). The corresponding impedance function can be computed as the quotient between the Fourier transforms of the output voltage $V_{out}(t, f)$ and the input current $I_{ZAP}(t)$, giving

$$Z(f) = \left|\frac{\mathcal{F}[V_{out}(t,f)](f)}{\mathcal{F}[I_{ZAP}(t)](f)}\right|. \tag{10}$$

For linear systems (7) (10) are equivalent. Note that eq. (8) can be thought of as a filtered version of the impedance function computed using the ZAP functions. ZAP currents are useful for some experimental purposes, but make strong assumptions about the underlying ionic process, particularly their time scales.

2.4 Phase-plane diagram for the autonomous system: nullclines

The V- and w-nullclines for system (1)-(2) are given, respectively, by

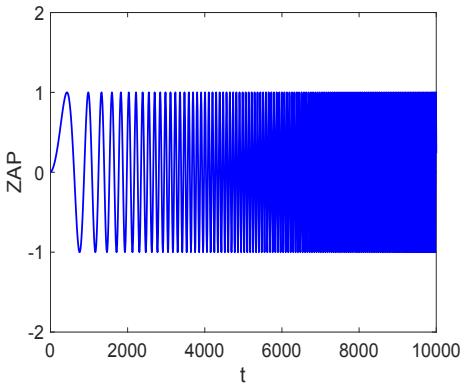

Figure 2: **Schematic diagram of a ZAP input.** We used (9) with $f_M = 100$, $T_M = 40000$ and $A_{in} = 0.1$. Only the first 10000 units of time are shown.

$$w = N_V(V) = \left(\frac{q-V}{R} + I\right) \frac{1}{p(V)} \tag{11}$$

and

$$w = N_w(V) = \left(1 - \frac{q-V}{R}\right) \frac{1}{1-\alpha\, p(V)} \tag{12}$$

If $q/R + I = 0$, then

$$w = N_V(V) = \frac{-1}{a_1 + a_2\, V + a_3\, V^2} = -\frac{1}{(V - V_{r,1})\,(V - V_{r,2})}, \tag{13}$$

where $V_{r,1}$ and $V_{r,2}$ are the roots of $p(V)$ if they exist. For the parameters we use [3,23,25] ($a_1 = 1.125$, $a_2 = -0.075$ and $a_3 = 0.00125$), $V_{r,1} = V_{r,2} = 30$ and therefore

$$w = N_V(V) = -\frac{1}{a_3\,(V-30)^2}. \tag{14}$$

Because the input function $I_{in}(t)$ varies between A_{in} and $-A_{in}$, this limits the values of A_{in} we can use to $A_{in} \leq q/R$.

Fig. 3 shows examples of the phase-plane diagrams for representative parameter values and $I = 0$, and Fig. 4 shows the nullclines for representative values of I. Additional cases were analyzed in [3].

2.5 Dynamic phase-plane analysis and extended phase-plane diagrams: "moving" nullclines

The forced system (1)-(2) is three-dimensional and the zero-level set for the first equation is two-dimensional (V-nullsurface). Following previous work [6, 7, 29, 30], we view the projections of this zero-level surface for increasing values of the input frequency f as a "moving" curve that we refer to as the "moving" V-nullcline. As time progresses, this V-nullcline (Fig. 5-c2, solid-red) moves cyclically in between the two curves corresponding to $\pm A_{in}$ (Fig. 5-c2, dashed-red), the maximum

and minimum values of the oscillatory input function $I_{in}(t)$, respectively, with a speed that depends on the input frequency f. The trajectory evolves following the motion of the V-nullcline targeting the fixed-point that locally governs the dynamics. The V-nullcline moves to the right (or up) in the ascending phase of the input and to the left (or down) in the descending phase of the input.

Fig. 6 illustrates this method in more detailed for the same parameter values used in Fig. 5-c2 and $f = f_{res} = 17$. Each snapshot corresponds to a time within one period after the response transients have worn off (tenth cycle using initial conditions close to the response cycle). The beginning of the cycle ($t = 0$) was chosen to be the time t at which $I_{in}(t) = 0$ and $I'_{in}(t) > 0$. At this time the V-nullcline is at baseline. The blue dot indicates the initial point of the trajectory ($t = 0$). As t progresses, the V-nullcline moves to the right (ascending phase) and the trajectory follows this motion and the motion of the "moving fixed-point" (intersection between the solid red and green curves), which is the target point for the trajectory. After the V-nullcline reaches its maximum level at $t = 250$ it moves back towards baseline, forcing the trajectory to reverse direction ($t = 350$). This process repeats and the trajectory reverses direction again after the V-nullcline reaches its lowest level ($t = 750$) and moves back towards baseline to close both the input and output cycles ($t = 1000$).

In order to simplify the analysis and aid in the comparison among the effects of different input frequencies, we will use an additional rescaling of the system (1)-(2) by defining

$$\hat{t} = \frac{t}{f}. \tag{15}$$

Substitution into (1)-(2) yields

$$\dot{V} = \frac{1}{f}\left[\frac{q-V}{R} - w\,p(V) + I_{in}(\hat{t}; f=1)\right] \tag{16}$$

and

$$\dot{w} = \frac{\epsilon}{f}\left[-\frac{q-V}{R} + 1 - w + \alpha\,w\,p(V)\right], \tag{17}$$

where the "dot" sign denotes derivative with respect to the new time $\hat{t}$. Unless necessary for clarity, we will drop the "hat" sign from $\hat{t}$.

This rescaling transforms the speed of the moving V-nullcline into a time scale for both equations. Specifically, the V-nullcline moves with the same speed for all input frequencies f, while the speed of the trajectories is f-dependent.

We note that the phase-plane diagrams extend to values of $w < 0$ and in some examples, the response limit cycles include values of $w < 0$. While this is not mathematically incorrect, these solutions do not represent realistic physical situations since concentrations cannot be negative. However, smaller values of the input amplitude will reduce the size of the limit cycle to include only values of $w > 0$ without changing the underlying mechanisms.

3 Results

3.1 Dynamics of the autonomous EC-cell

The effects of changes in the values of the model parameters (q, α and R) on the dynamics of the EC model (1)-(2) in the absence of any external input ($I_{in} = 0$) has been thoroughly investigated in [3].

Additional aspects of the model have been studied in [23, 25]. We briefly discuss here a few cases relevant for the focus of this paper. The phase-plane diagrams in Fig. 3 show that for low enough values of q, the EC model has a single fixed-point that is a stable node (Figs. 3-a1 and -b1). For larger values of q, the fixed-points are stable foci (Fig. 3-a2, -a3, -b2 and -b3). The critical values of q for the transition between stable nodes and foci depende on the other model parameters (compare Figs. 3-a and -b). For higher values of q than these showed in Figs. 3 the system develops limit cycles and multiple fixed-points that in some cases may lead to bistability. We refer the reader to [3] for more details and information. In this paper we focus on the parameter regime where the autonomous system ($I_{in} = 0$) has a single stable fixed-point.

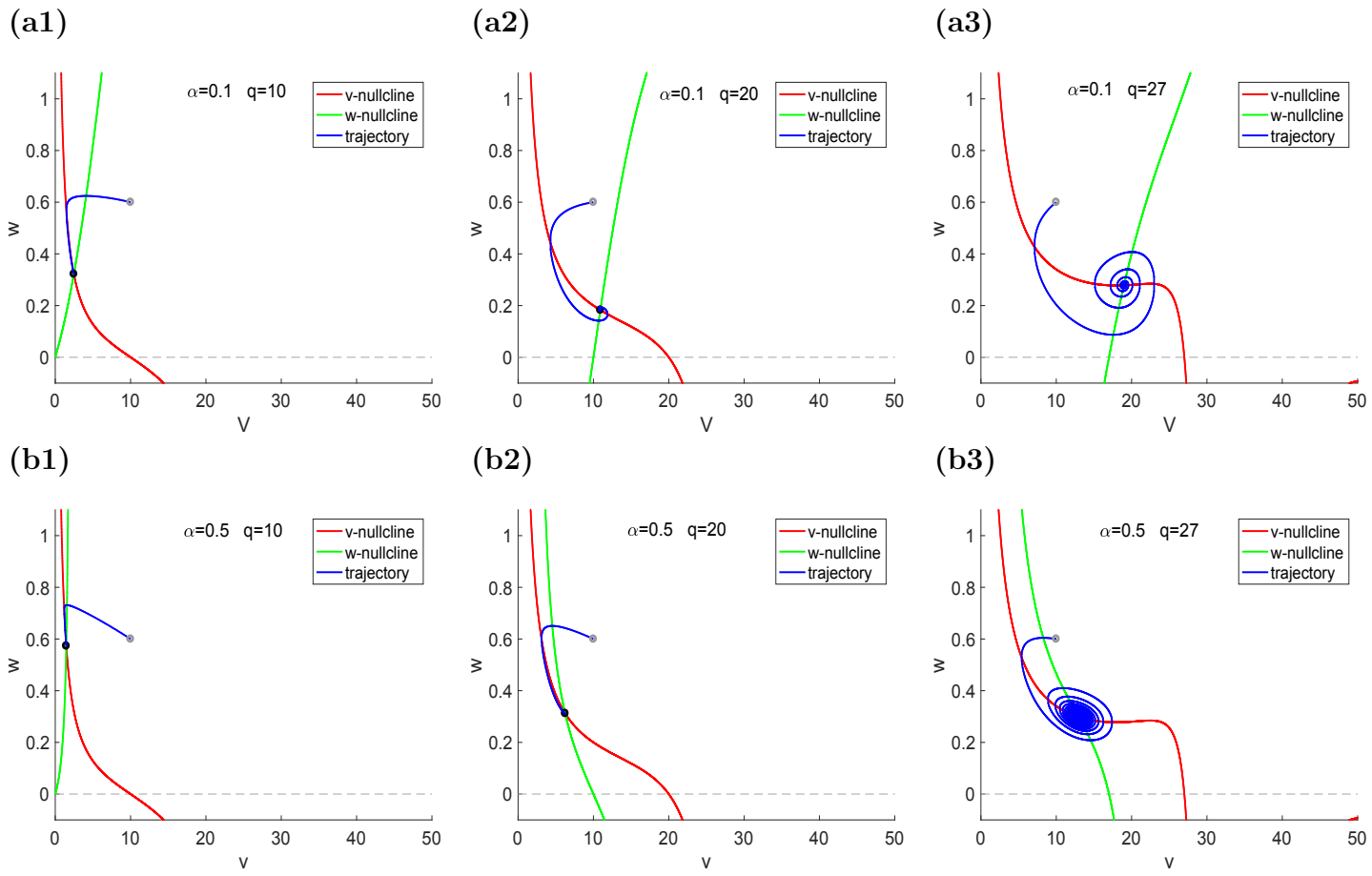

Figure 3: **Phase-plane diagrams for the autonomous system for representative parameter values. (a)** $\alpha = 0.1$. **(a1)** $q = 10$. The fixed-point is a stable node. The eigenvalues are $r_1 = -0.0524$ and $r_2 = -0.3210$ (stable node). **(a2)** $q = 20$. The fixed-point is a stable focus. The eigenvalues are $r_{1,2} = -0.0515 \pm i\,0.1158$ (stable focus). **(a3)** $q = 27$. The fixed-point is a stable focus. The eigenvalues are $r_{1,2} = -0.009 \pm i\,0.0872$ (stable focus). **(b)** $\alpha = 0.5$. **(b1)** $q = 10$. The fixed-point is a stable node. The eigenvalues are $r_1 = -0.0351$ and $r_2 = -0.5961$ (stable node). **(b2)** $q = 20$. The fixed-point is a stable focus. The eigenvalues are $r_{1,2} = -0.0842 \pm i\,0.0752$ (stable focus). **(b3)** $q = 27$. The fixed-point is a stable focus. The eigenvalues are $r_{1,2} = -0.0014 \pm i\,0.0914$ (stable focus). We used the following parameter values: $\epsilon = 0.03$, $R = 10$ and $I = 0$.

The input current I_{in} can be thought as continuously changing the shape of the V-nullcline (11), but not the shape of the w-nullcline (12). To begin to understand this effect, Fig. 4 illustrates the effect of constant values of I on the shape of the V-nullcline. As discussed in Section 2.4, the V-nullcline can be rewritten as

$$w = N_V(V) = -(q - V + R\,I)\,\frac{1}{a_3\,V\,(V-30)^2\,R}. \tag{18}$$

It has two vertical asymptotes at $V = 0$ and $V = 30$. From (18), $N_V > 0$ ($N_V < 0$) if $V < q + RI$ ($V > q + RI$). For $I = 0$ (baseline), $N_V > 0$ ($N_V < 0$) if $V < q$ ($V > q$) (Fig. 4, solid curves). Increasing values of I increase the range of values of V for which $N_V > 0$. For low enough values of $I > 0$ the V-nullcline is displaced from, but qualitatively similar to baseline (Figs. 4-a1 and -b1, dashed-red), while for high enough values of $I > 0$ there is a qualitative change in the shape of the V-nullcline that becomes parabolic-like on the left side to the vertical asymptote (Figs. 4-a1 and -b1, dashed-dotted-red). The transition point between the qualitatively different shapes depends on the other parameter values. For negative values of I the V-nullcline is displaced to the left (not shown). Note that as the result of changes in I, not only the fixed-points change their location, but additional fixed-points are created. We leave the analysis of the stability of these fixed-points out of this study, since they are not actual fixed-points of the forced system.

3.2 Dynamic mechanisms of generation of resonance

The dynamic mechanism of generation of resonance has been throughly investigated in [6] for linear systems and extended for nonlinear systems of quadratic type in [7] (see also [29, 30]). In these papers [6, 7] we focused particularly on systems that exhibit resonance but not oscillations (not even damped oscillations) [3, 5]. Because the eigenvalues are not necessarily complex, and therefore the system may have zero natural frequency, the of resonance must not be associated to the natural frequency of the autonomous system and the mechanism responsible for the generation of resonance must be explained without resorting to any property of intrinsic oscillations.

In [6, 7] we develop dynamical systems tools to investigate the resonance phenomena without the need to resort to complex eigenvalues and eigenvectors. We extend these tools here to investigate the resonant properties of the EC model subject to the frequency rescaling described in Section 2.5, given by equations (16)-(17).

Fig. 5 show representative examples of the resonant response of the EC model to sinusoidal inputs. For $A_{in} = 0$ the system has a stable node. For low values of A_{in} the response is quasi-linear (Figs. 5-a and -b, blue). For higher values of A_{in} the response is nonlinear (Figs. 5-a and -b, red), characterized by a lack of proportionality with increasing values of A_{in} and the lack of symmetry in the envelope response. Fig. 5-c1 shows representative V-traces (curves of V versus time) for $A_{in} = 1$ (red curves in panels a and b). Fig. 5-c2 shows the extended phase-plane diagram. The dashed-red curves correspond to the V-nullcline (11) for $I = \pm A_{in} = \pm 1$. The V-nullcline moves cyclically in between these two curves. As this happens the fixed-point also moves along the w-nullcline. The trajectory evolves following these dynamics of the V-nullcline, targeting the fixed-point.

For values of $f \to 0$ (particularly, $f < \epsilon$) the dynamics is infinitely fast and the trajectory follows the motion of the fixed-point, evolving along the w-nullcline. For higher, but still small values of f, the trajectory moves quasi-elliptically around the w-nullcline in between the intersections between the w-nullcline and the dashed-red curves (Fig. 5-c2, $f = 1$). The maximum values of V for $f = 0$, $V_{max}(0)$,

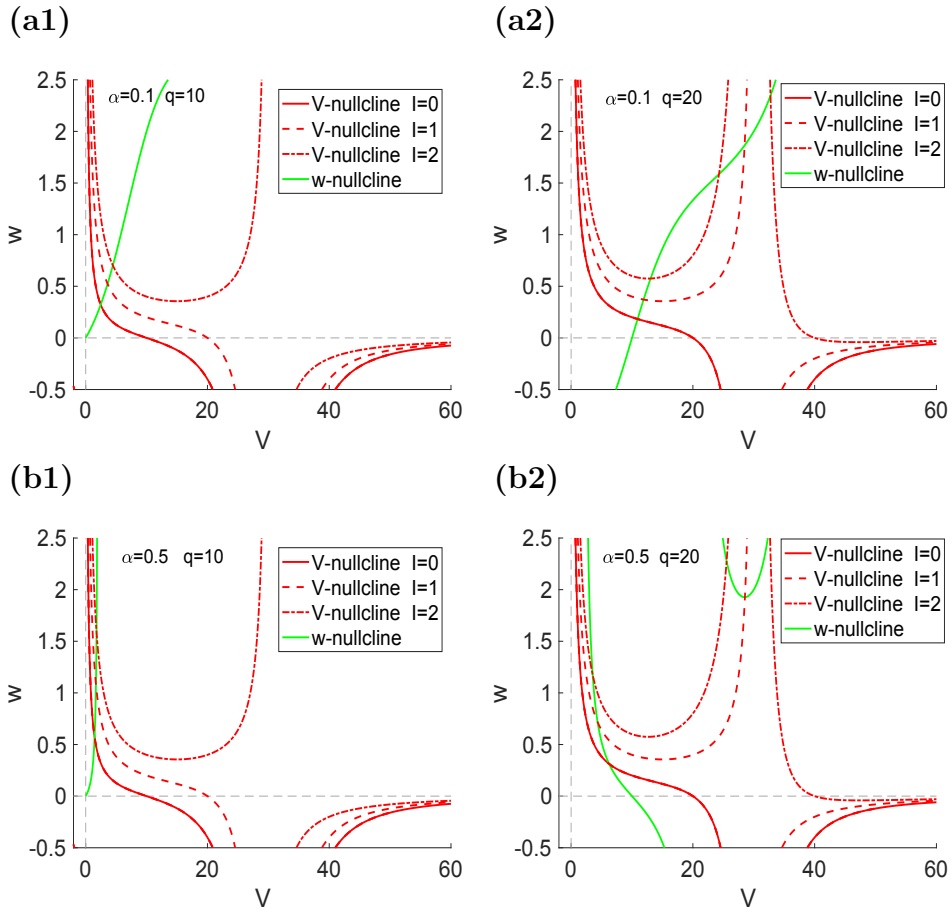

Figure 4: **Nullclines for the autonomous system for representative parameter values: dependence on I. (a)** $\alpha = 0.1$. **(a1)** $q = 10$. **(a2)** $q = 20$. **(b)** $\alpha = 0.5$. **(b1)** $q = 10$. **(b2)** $q = 20$. We used the following parameter values: $\epsilon = 0.03$ and $R = 10$.

corresponds to the V-coordinate of this intersection. On the other extreme, for large enough values of f, the evolution of the trajectory is very slow and it cannot reach long enough distances before the V-nullcline "comes back" and causes the trajectory to reverse direction (Fig. 5-c2, $f = 100$). In the limit $f \to \infty$ the trajectory remains at the fixed-point ($V_{max}(f) \to 0$).

For intermediate values of f the shapes of the limit cycle responses transitions in between these two limiting cases. They first widen and then shrink. From this geometric perspective, the system exhibits resonance if $V_{max}(f)$, the maximum value of V on the limit cycle response, satisfies $V_{max}(f_{res}) > V_{max}(0)$ (Fig. 5-c2, $f = f_{res} = 17$). From this geometric point of view, the response limit cycle trajectory has "more freedom" of motion for f_{res} than for the other frequencies, particularly for $f = 0$ and $f \to 0$ that are constrained to evolve in quasi-one-dimensional regions. The relative speed between the moving V-nullcline and the limit cycle trajectory for f_{res} is optimal in the sense that is neither too fast nor to slow so that the voltage response is able to reach longer distances in the V-direction than the other input frequencies before it intersects the moving V-nullcline and is forced to reverse direction. This intersection occurs the moving V-nullcline reaches its highest level (Fig. 6, $t = 250$). Because the intersection between the trajectory and the moving nullcline cannot occur further up (or further to the right) than the highest level, for all other frequencies the maximum V values the trajectory reaches cannot be higher than for the resonant frequency.

The geometric properties of the nullclines, particularly the V-nullcline play a significant role in shaping the system's frequency-dependent response to oscillatory inputs. For example, the almost vertical displace V-nullcline in Fig. 5-c2 (dashed-red, left) causes the lower envelope in Fig. 5-a (red) to be low-pass filter instead of a high-pass filter as the upper envelope (see also Fig. 6, $t = 750$ and $t = 850$). For lower values of A_{in} (e.g., Fig. 5-a, blue for $A_{in} = 0.1$) the lower envelope is a band-pass filter since the shape of the displaced V-nullcline is closer to the shape of the actual V-nullcline (solid-red) (not shown).

We use this approach to understand the relationship between the model parameters, encoded by the nullclines, and the model response properties to oscillatory inputs, particular the resonance phenomenon in the presence of model nonlinearities.

3.3 Nonlinear dependence of the V-response: nonlinear resonance

The mechanism of generation of resonance has been described in Section 3.2 and illustrated in Fig. 6. Linear systems are characterized by a few properties: (i) uniformity of the steady state response across cycles, (ii) coincidence of the output and input frequencies, (ii) proportionality between the output and the input, (iii) symmetry of the output with respect to the equilibrium value around which the system s perturbed. The response in Fig. 5 for $A_{in} = 0.1$ (blue) is quasi-linear. Although the nullclines are non-linear, particularly the V-nullcline, its displacement from baseline is very small (not shown), thus not allowing the response trajectory to move away from the quasi-linear regime. The displacement of the V-nullclines from baseline for $A_{in} = 1$ is larger (Fig. 5-c2), leading to a nonlinear response (Fig. 5-a, red), which is characterized primarily by the lack of symmetry between the upper and lower envelopes. Note that the Z-profiles (Fig. 5-b) show a quasi-linear response (compare the red and blue Z-profiles), indicating that they do not necessarily capture the effects of the nonlinearities.

Fig. 7 shows the results for the same parameter values as in Fig. 5, but a higher value of q ($q = 20$). This higher value of q allows for higher values of A_{in}. For low enough values of A_{in} the response is quasi-linear (Fig. 7-a, blue) as in the previous case. As A_{in} increases, asymmetries in the response envelopes begin to develop (Fig. 7-a, red and green) and the changes in the impedance profiles do not

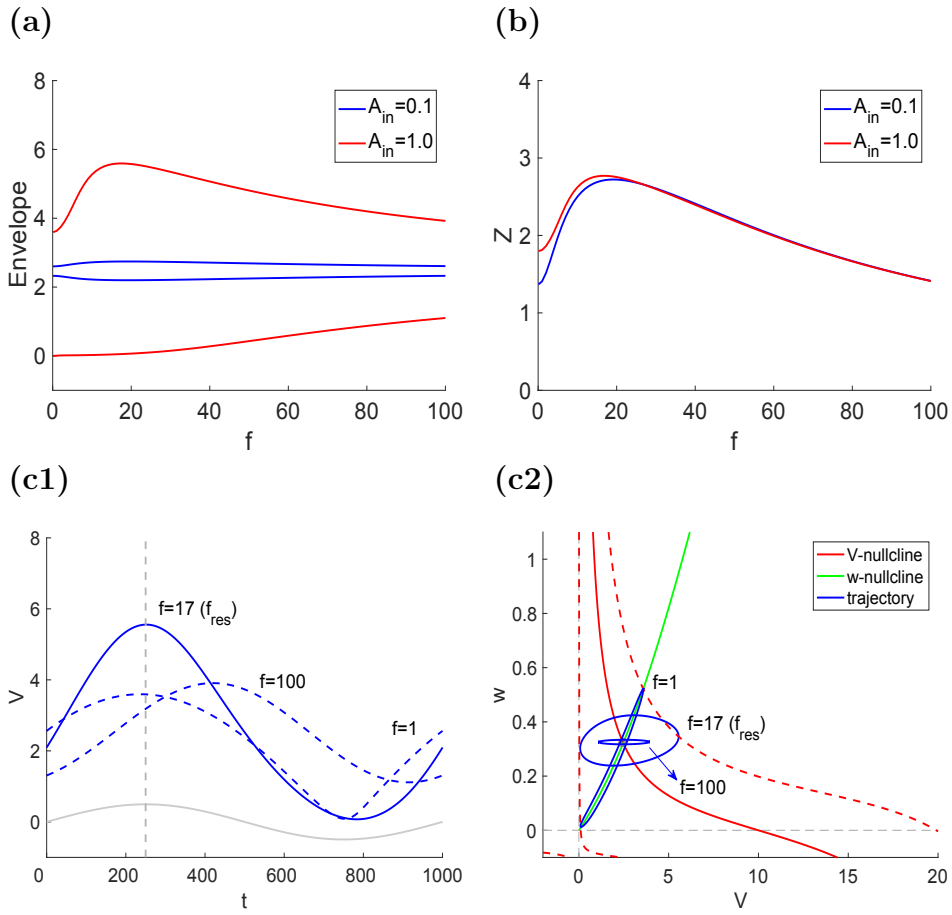

Figure 5: **Response of the EC-cell to oscillatory input currents.** **(a)** Voltage envelope response. The upper and lower curves correspond to the steady state maximum (V_{max}) and minimum (V_{min}) values of V for each input frequency f. **(b)** Impedance profile. It was computed using (8). **(c1)** Voltage traces for $A_{in} = 1$ (red curves in panels a and b) and representative values of the input frequency f. The vertical dashed-gray curve indicates the peak of the oscillatory input (solid-gray, caricature) **(c2)** Extended phase-plane diagram for $A_{in} = 1$ (red curves in panels a and b) and representative values of the input frequency f. The dashed-red curves are the V-nullclines for I substituted by $A_{in} = 1$ (upper) and $A_{in} = -1$ (lower). We used the following parameter values: $\epsilon = 0.03$, $\alpha = 0.1$, $R = 10$ and $q = 10$.

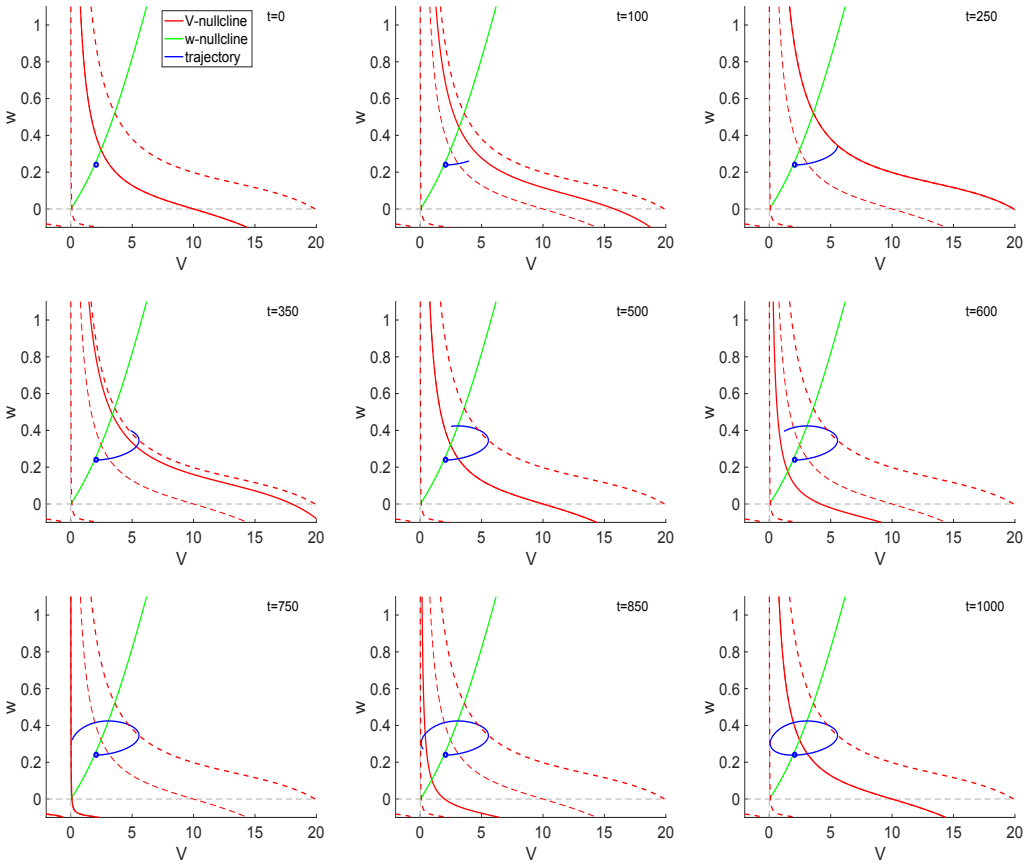

Figure 6: **Snapshots of the evolution of the (stationary) response trajectory in the extended phase-plane diagram for $f = f_{res} = 17$ in Fig. 5-c2.** The blue dot indicates the location of the trajectory at $t = 0$ (beginning of the cycle for which $I_{in}(t) = 0$ and $I'_{in}(t) > 0$). The trajectory's endpoint corresponds to the indicated time. The solid-red curve represents the "moving" V-nullcline at the indicated time. The thicker dashed-red curves are the V-nullclines for I substituted by A_{in} (upper) and $-A_{in}$ (lower). The slimmer dashed-red curve is the baseline V-nullcline ($I_{in}(t) = 0$). We used the following parameter values: $A_{in} = 1$, $\epsilon = 0.03$, $\alpha = 0.1$, $R = 10$ and $q = 10$.

change proportionally with A_{in} (Fig. 7-b).

Comparison between Figs. 5-a and 7-a shows that for the same values of A_{in} (blue and red curves in both figures) the responses are stronger the larger the value of q (stronger in Fig. 7-a than in Fig. 5-a), particularly in vicinities of the resonant frequency. This is mainly due to the qualitative differences in the geometric properties of the extended phase-plane diagram between the two cases ($q = 10$ and $q = 20$). More specifically, as we discussed in Section 3.1, it is due to the the qualitative differences in the effect that the input has on the shapes of the V-nullclines between the two cases, reflected by the extended V-nullclines (dashed-red). For $A_{in} = 1$, the parabolic-like shape of the extended V-nullclines for $q = 20$ (Fig. 7-c2) allows the response trajectory for frequencies close to the resonant frequency to reach larger distances (in the V direction) than for $q = 10$ (Fig. 5-c2). This effect is magnified for $q = 20$ and $A_{in} = 2$ (Fig. 5-d2), thus producing a stronger response as can be seen by comparing the extended phase-plane diagrams in Figs. 6 and 8.

The combination of the nonlinearities and the time scale separation induced by ϵ affect the waveform of the response for frequencies close to the resonant frequency, which is sinusoidal-like for $A_{in} = 1$ (Fig. 7-c1) and relaxation-like for $A_{in} = 2$ (Fig. 7-c2).

In Fig. 9 we show the envelope responses (left panels) and the impedance profiles (right panels) computed using the ZAP input (9) and (10). Comparison with Figs. 5 and 7 shows that the results using the two approaches are consistent for $q = 10$ (Figs. 5-a1 and 9-a1) with a slighter nonlinear amplification of the response for the ZAP approach. For $q = 20$, the envelope results are consistent between the two approaches (Figs. 7-a1 and 9-b1), but the impedance profile results are somehow contradictory (Figs. 7-a2 and 9-b2). Fig. 7-a2 shows an attenuation of the response, while Fig. 9-b2 shows an amplification of the response. These differences are likely to be due to the fact that, because of its nature, the ZAP approach captures transient effects, which are almost absent in the other, steady-state-based approach.

3.4 Nonlinear dependence of the V-response: mixed-mode amplitude patterns

Fig. 10 shows the envelope responses (left panels) and the impedance profiles (right panels) computed using the ZAP input (9) and (10) for a higher value of α ($\alpha = 0.5$) than in the previous figures and the two values of q we used before: $q = 10$ (Fig. 10-a) and $q = 20$ (Fig. 10-b). The response patterns for $A_{in} = 0.1$ (blue curves) and $A_{in} = 1$ (red curves) are similar to these for $\alpha = 0.1$ (Fig. 9-a), but more attenuated. In contrast, the response patterns for $A_{in} = 2$ (green curves) are qualitatively different from these for $\alpha = 0.1$. The envelope response (Fig. 10-b1) shows a range of frequencies with two maxima, indicating the presence of patterns with two steady state oscillatory amplitudes that alternate across cycles. This split is also captured by the envelope patterns computed using a sequence of sinusoidal inputs at different frequencies and (8) (Fig. 11-a). The impedance profile in Fig. 10-b2 (green) captures these patterns by showing a second peak at a frequency higher than the resonant frequency. However, note that this type of second peak may also be present due to the shape of uniform oscillatory patterns.

Figs. 11-c1 and -d1 illustrates the oscillatory response pattern for $f = f_{res} = 9$ (c1, solid), whose amplitude is the same across cycles, and $f = 20$ (d1, solid) that has two alternating characteristic amplitudes. The extended phase-plane diagrams in Figs. 11-c2 and d2 show that while the cycles for the uniform response patterns (e.g., $f = 9$) are simple closed curves, the cycles for the non-uniform response patterns (e.g., $f = 20$) have loops.

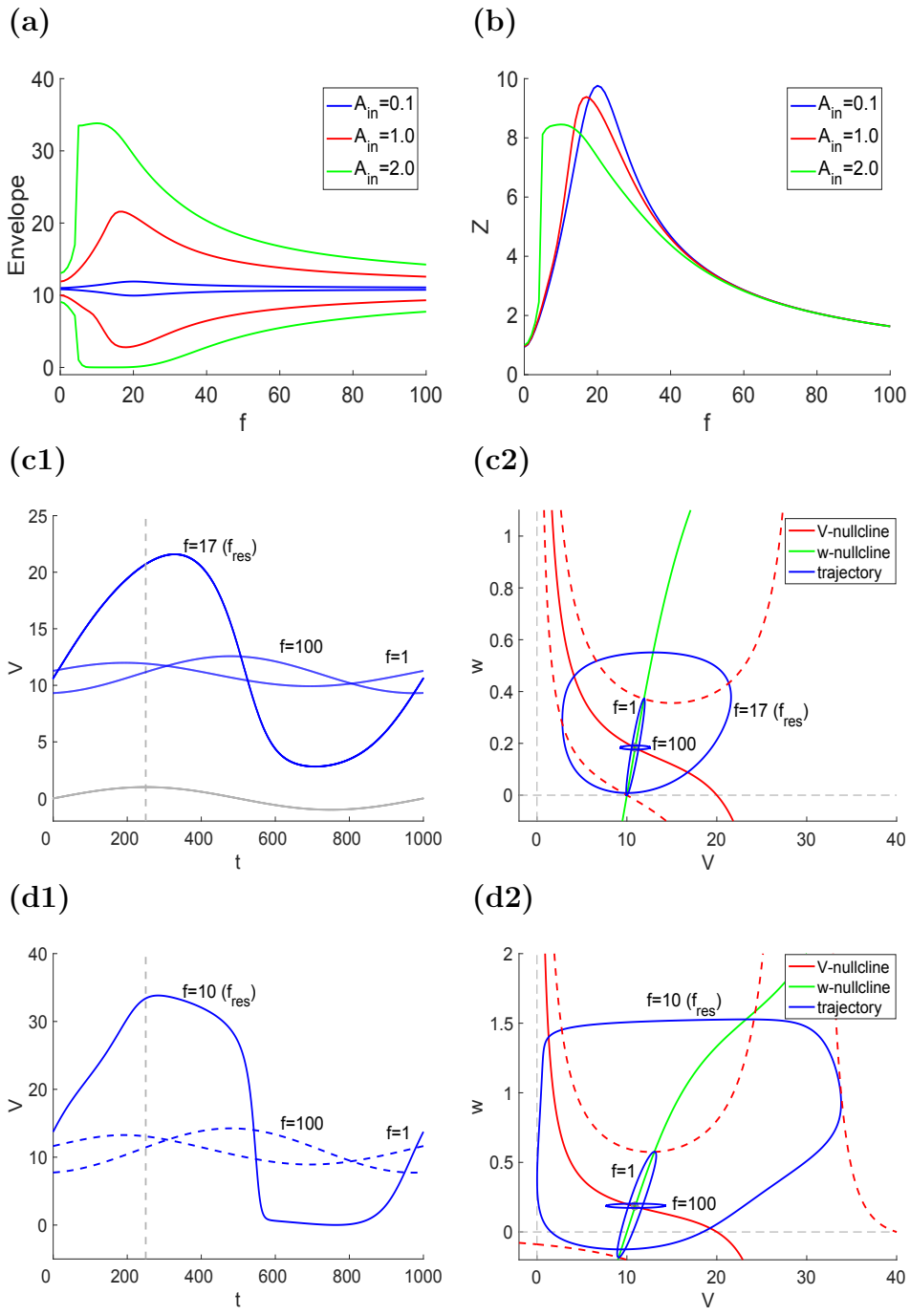

Figure 7: **Response of the EC-cell to oscillatory input currents.** **(a)** Voltage envelope response. The upper and lower curves correspond to the steady state maximum (V_{max}) and minimum (V_{min}) values of V for each input frequency f. **(b)** Impedance profile. It was computed using (8). **(c1,d1)** Voltage traces for $A_{in} = 1$ (c1, red curves in panels a and b) and $A_{in} = 2$ (d1, green curves in panels a and b) and representative values of the input frequency f. The vertical dashed-gray curve indicates the peak of the oscillatory input (solid-gray, caricature) **(c2,d2)** Extended phase-plane diagram for $A_{in} = 1$ (c1, red curves in panels a and b) and $A_{in} = 2$ (d1, green curves in panels a and b) and representative values of the input frequency f. The dashed-red curves are the V-nullclines for I substituted by $A_{in} = 1$ (upper) and $A_{in} = -1$ (lower). We used the following parameter values: $\epsilon = 0.03$, $\alpha = 0.1$, $R = 10$ and $q = 20$.

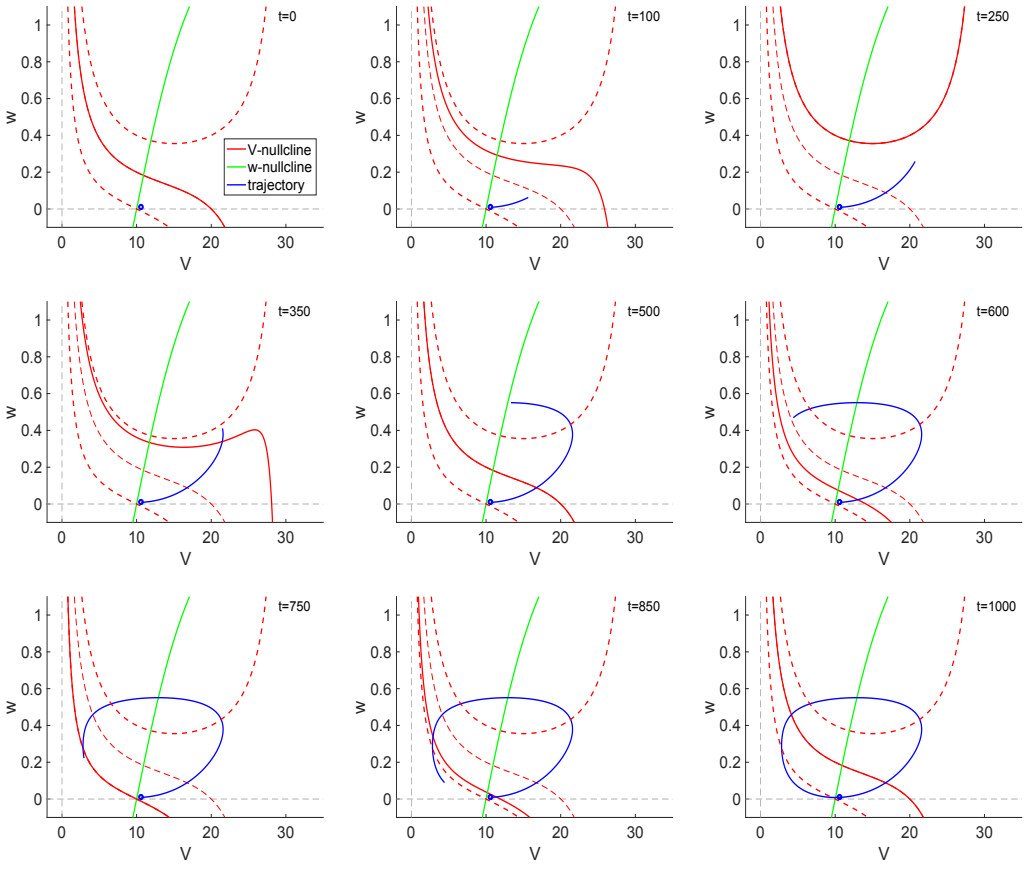

Figure 8: **Snapshots of the evolution of the (stationary) response trajectory in the extended phase-plane diagram for $f = f_{res} = 17$ in Fig. 7-c2.** The blue dot indicates the location of the trajectory at $t = 0$ (beginning of the cycle for which $I_{in}(t) = 0$ and $I'_{in}(t) > 0$). The trajectory's endpoint corresponds to the indicated time. The solid-red curve represents the "moving" V-nullcline at the indicated time. The thicker dashed-red curves are the V-nullclines for I substituted by A_{in} (upper) and $-A_{in}$ (lower). The slimmer dashed-red curve is the baseline V-nullcline ($I_{in}(t) = 0$). We used the following parameter values: $A_{in} = 1$, $\epsilon = 0.03$, $\alpha = 0.1$, $R = 10$ and $q = 20$.

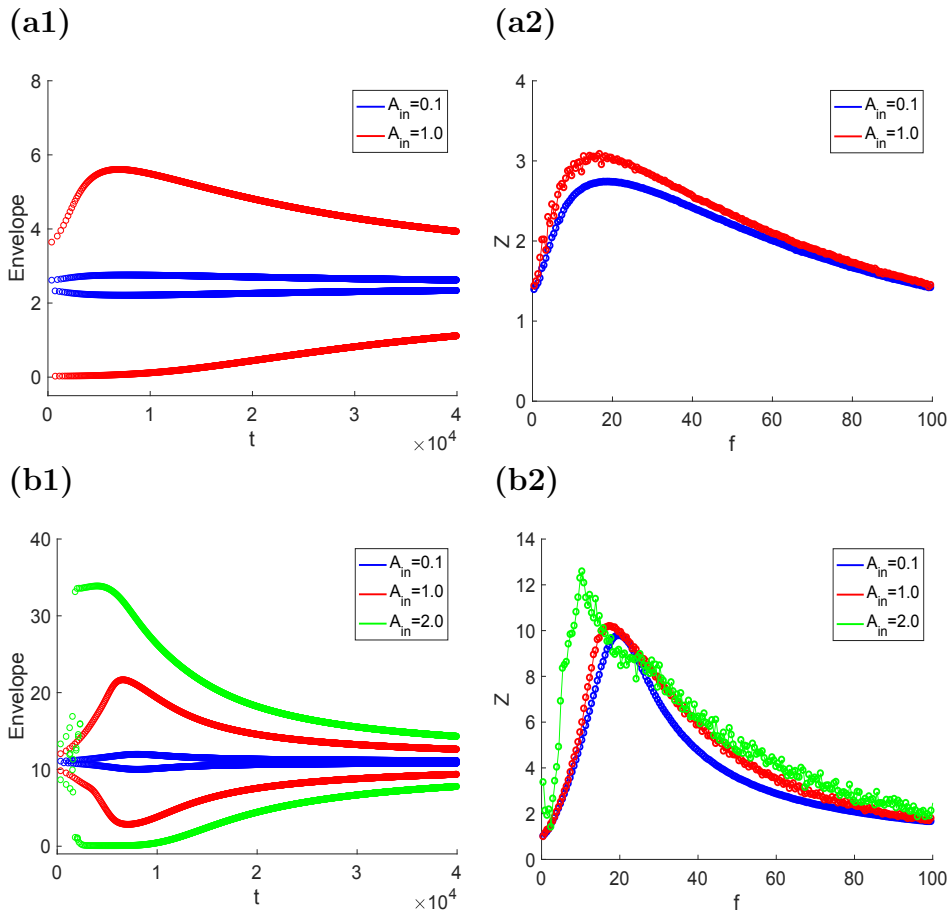

Figure 9: **Response of the EC-cell to oscillatory ZAP input currents** ($\alpha = 0.1$)**.** The ZAP input current is given by (9) with $f_M = 100$, $T_M = 40000$ and $A_{in} = 0.1$ (Fig. 2). **Left panels.** Envelope response. Each point in the upper and lower curves is a response peak and trough, respectively. **Right panels.** Impedance profiles. They were computed using (10). **(a)** $q = 10$ (same as Fig. 5). **(b)** $q = 20$ (same as Fig. 7). We used the following parameter values: $\epsilon = 0.03$, $\alpha = 0.1$ and $R = 10$.

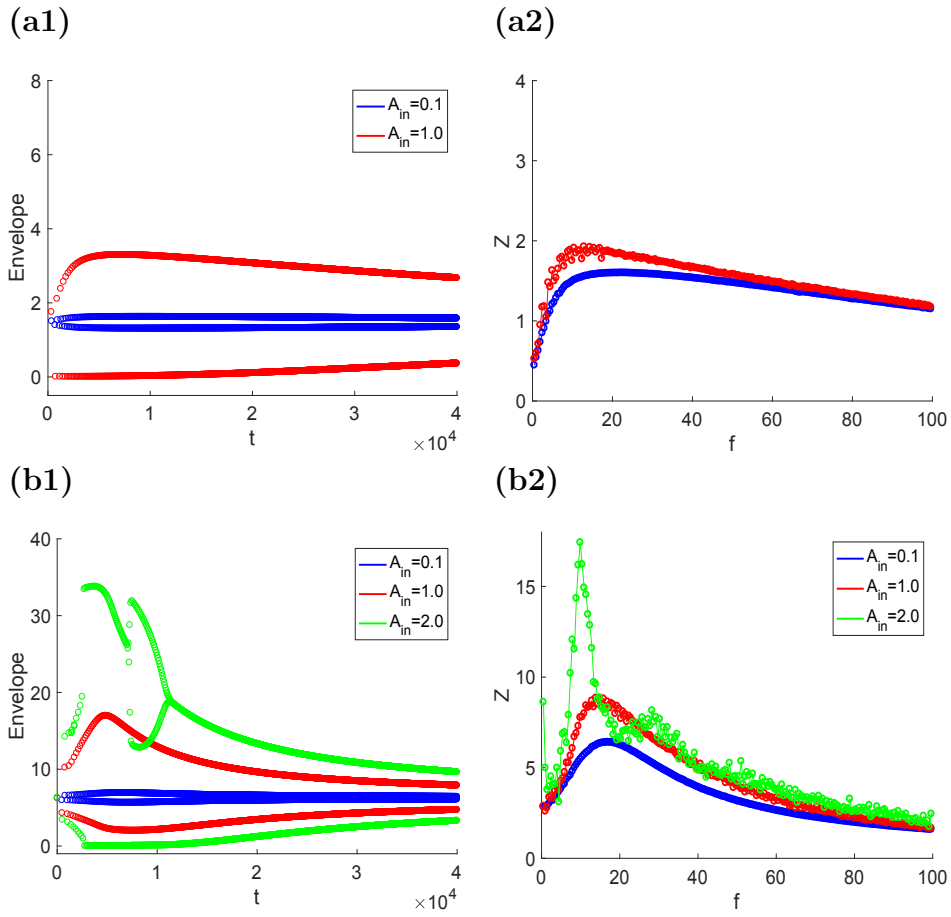

Figure 10: **Response of the EC-cell to oscillatory ZAP input currents** ($\alpha = 0.5$)**.** The ZAP input current is given by (9) with $f_M = 100$, $T_M = 40000$ and $A_{in} = 0.1$ (Fig. 2). **Left panels.** Envelope response. Each point in the upper and lower curves is a response peak and trough, respectively. **Right panels.** Impedance profiles. They were computed using (10). **(a)** $q = 10$. **(b)** $q = 20$. We used the following parameter values: $\epsilon = 0.03$, $\alpha = 0.5$ and $R = 10$.

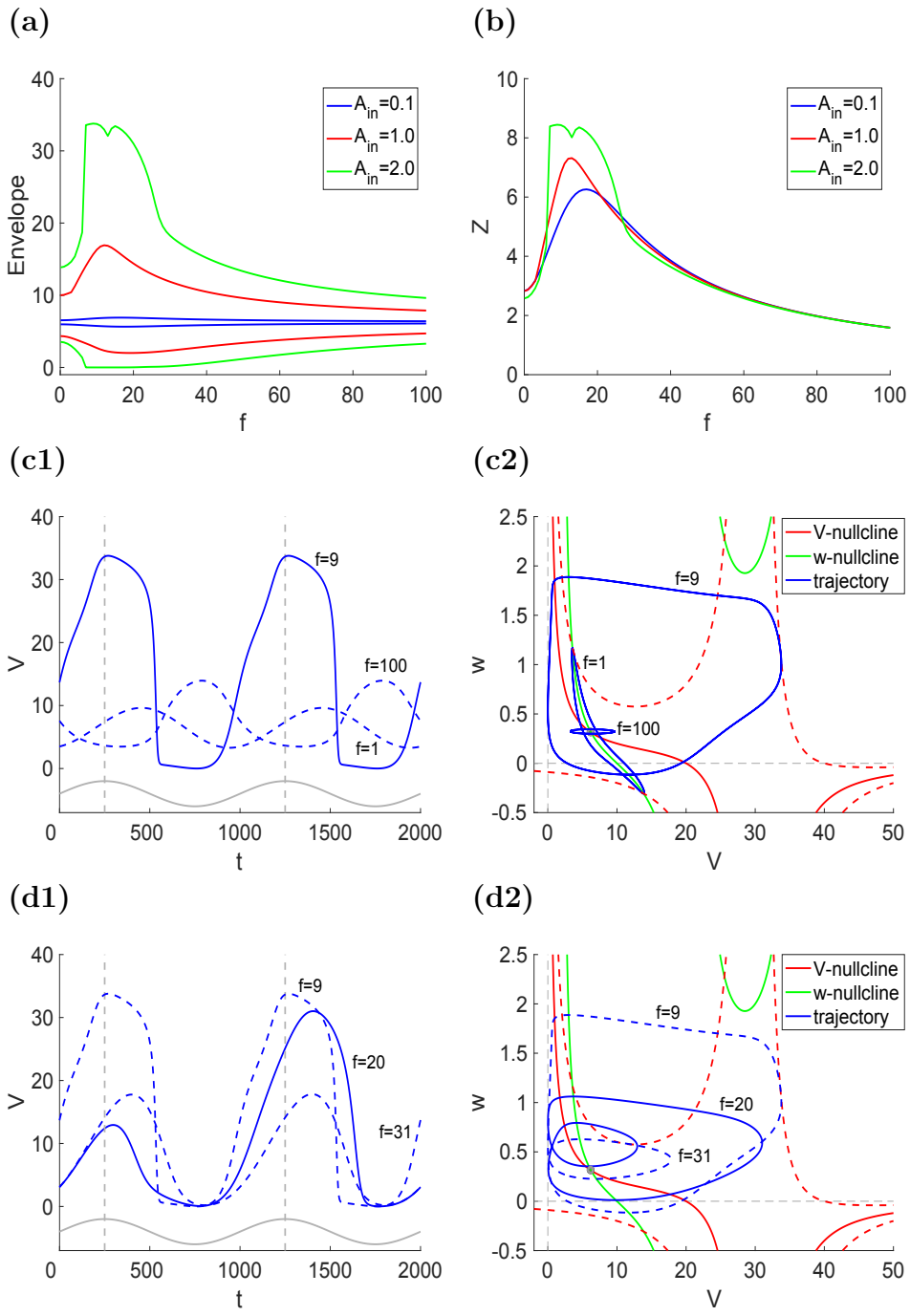

Figure 11: **Response of the EC-cell to oscillatory input currents ($\alpha = 0.5$ and $q = 20$). (a)** Voltage envelope response. The upper and lower curves correspond to the steady state maximum (V_{max}) and minimum (V_{min}) values of V for each input frequency f. **(b)** Impedance profile. It was computed using (8). **(c1,d1)** Voltage traces for $A_{in} = 2$ (c1, red curves in panels a and b) and $A_{in} = 2$ (d1, green curves in panels a and b) and representative values of the input frequency f. The vertical dashed-gray curve indicates the peak of the oscillatory input (solid-gray, caricature) **(c2,d2)** Extended phase-plane diagram for $A_{in} = 2$ (c1, red curves in panels a and b) and $A_{in} = 2$ (d1, green curves in panels a and b) and representative values of the input frequency f. The dashed-red curves are the V-nullclines for I substituted by $A_{in} = 1$ (upper) and $A_{in} = -1$ (lower). We used the following parameter values: $\epsilon = 0.03$, $\alpha = 0.5$, $R = 10$ and $q = 20$.

We analyze the differences between these two cases using the extended phase-plane diagrams in Figs. 12 ($f = 9$) and 13 ($f = 20$). Although there a differences in the extended phase-plane diagrams due to the different parameter values, the dynamics for $f = 9$ (Figs. 12) is qualitatively similar to those in Fig. 8, except that the intersection between the trajectory and the moving V-nullcline in its ascending phase occurs at its right-most branch instead that on the parabolic-like branch ($t = 250$). This causes the response amplitude to be larger in Fig. 12 than in Fig. 8.

The dynamics are qualitatively different for $f = 20$ (Fig. 13). The first intersection between the trajectory and the moving V-nullcline occurs on its parabolic-like branch ($t = 250$). This causes the trajectory to reverse direction ($t = 350$). Because of the shape of the V-nullcline and the timing, after the second intersection ($t = 850$, descending phase) the trajectory moves almost vertically and turns around at a lower level than the initial point ($t = 1000$) and the cycle cannot be closed and a second "round" is initiated. The second intersection between the trajectory and the moving V-nullcline (ascending phase) occurs at the right-most branch ($t = 1350$). After reversing direction and intersecting the V-nullcline again ($t = 1850$, descending phase) at a higher level than the previous time, the trajectory closes the loop.

4 Discussion

Electrochemical (EC) systems have been shown to produce complex response patterns to oscillatory inputs [1, 3, 10–18, 21, 22, 31]. Previous modeling efforts have focused on the analysis of linearized models and numerical simulations of nonlinear models with various degrees of complexity. To our knowledge, no existing study has addressed the combined nonlinear dynamic and mechanistic aspects of the responses of EC cells to oscillatory inputs.

We set out to investigate how the nonlinearities generated by the physicochemical properties of the EC cells shape their dynamic response to oscillatory inputs. We used a phenomenological model that is simple enough to be amenable for analysis using dynamical systems tools, but it includes the necessary physicochemical complexity to make the results relevant for the understanding of the more realistic and complex models. While our caricature model is not realistic in the sense that it cannot be experimentally implemented without the appropriate modifications, it is helpful to understand th relationship between the model nonlinearities and the response patterns in a relatively straightforward way. Caricature and reduced models have been used in the literature for this type of purpose with successful results [26, 27, 32, 33]. The results obtained from toy models are typically representative of a larger class of models. Therefore we expect the results of our study can serve as a guide for similar studies using more realistic models and the tools we develop in this paper can be used and adapted to understand these patterns.

For simplicity, we used an additive current and we focus on a regime where the unforced system has a single stable equilibrium point (node or focus). The model nonlinearities are captured by the nullclines. The baseline nonlinearities (the nonlinearities for the unforced system) are relatively simple. The V-nullclines are monotonically decreasing functions of V and the w-nullclines are quasi-linear in large enough vicinities of the fixed-points. The nonlinearities that effectively control the response dynamics become more pronounced as the input amplitude increases. The moving V-nullclines transition from baseline to cubic-like, parabolic-like and in some cases an additional branch is developed for relatively high values of V. As this happens not only the fixed-point moves in the extended phase-plane diagram, but additional fixed-points are created and destroyed. Although these are not actual

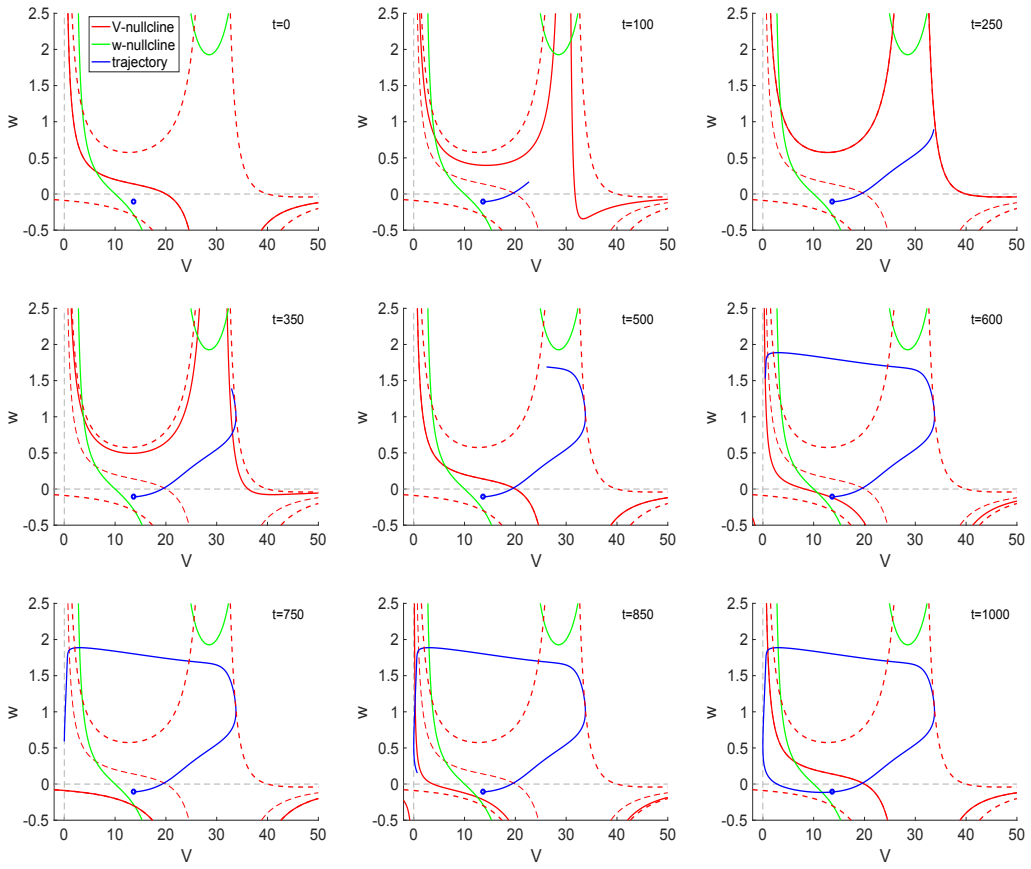

Figure 12: **Snapshots of the evolution of the (stationary) response trajectory in the extended phase-plane diagram for $f = 9$ in Fig. 11-c2.** The blue dot indicates the location of the trajectory at $t = 0$ (beginning of the cycle for which $I_{in}(t) = 0$ and $I'_{in}(t) > 0$). The trajectory's endpoint corresponds to the indicated time. The solid-red curve represents the "moving" V-nullcline at the indicated time. The thicker dashed-red curves are the V-nullclines for I substituted by A_{in} (upper) and $-A_{in}$ (lower). The slimmer dashed-red curve is the baseline V-nullcline ($I_{in}(t) = 0$). We used the following parameter values: $A_{in} = 2$, $\epsilon = 0.03$, $\alpha = 0.5$, $R = 10$ and $q = 20$.

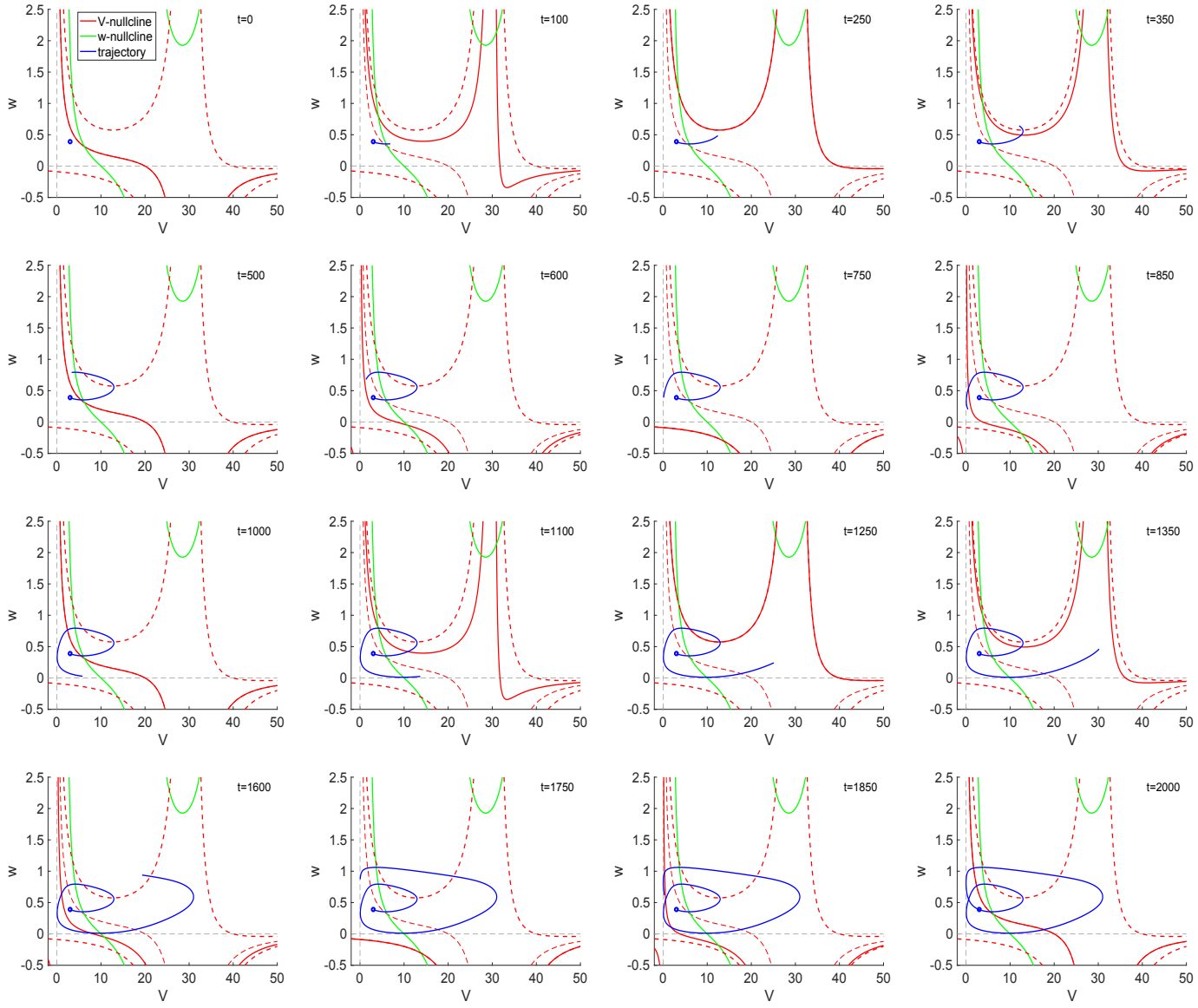

Figure 13: **Snapshots of the evolution of the (stationary) response trajectory in the extended phase-plane diagram for $f = 20$ in Fig. 11-d2.** The blue dot indicates the location of the trajectory at $t = 0$ (beginning of the cycle for which $I_{in}(t) = 0$ and $I'_{in}(t) > 0$). The trajectory's endpoint corresponds to the indicated time. The solid-red curve represents the "moving" V-nullcline at the indicated time. The thicker dashed-red curves are the V-nullclines for I substituted by A_{in} (upper) and $-A_{in}$ (lower). The slimmer dashed-red curve is the baseline V-nullcline ($I_{in}(t) = 0$). We used the following parameter values: $A_{in} = 2$, $\epsilon = 0.03$, $\alpha = 0.5$, $R = 10$ and $q = 20$.

fixed-points in the strict sense, they organize the dynamics of the perturbed system by transiently become the target of the response trajectories.

The classical measure of resonance assumes that the number of stationary output cycles have uniform amplitude. For linear models, the number of input and output cycles coincide, the output envelope response is symmetric with respect to the horizontal line representing the V-coordinate of the fixed-point, and the amplitude of the output response is proportional to the input amplitude. Our results show that resonances can be nonlinearly amplified or attenuated depending on the input amplitude and the model parameters regime. This is the result of the response trajectories for the resonant frequency crossing the moving V-nullclines at levels where the latter are qualitatively different from the baseline V-nullcline (e.g., parabolic-like vs. quasi-linear), and therefore the behavior departs from the linear prediction in different ways. Our results also show parameter regimes where the response patterns are of mixed-mode type, whose stationary amplitude is not uniform across cycles, but there are two characteristic, alternating amplitudes, captured by a loop in the response cycle in the extended phase-plane diagram. This amplitude split is the result of a timing mechanism that causes the response cycle trajectory to cross different branches of the moving V-nullcline in the extended phase-plane diagram in response to subsequent input cycles for a range of input frequencies. None of these response patterns are captured by the linearized models investigated in previous work [3]. Additional, more complex response patterns are expected in other parameter regimes, particularly these closer to the Hopf bifurcation for the generation of sustained oscillations.

The impedance profile does not necessarily capture the response dynamics. This is better captured by the envelope response profiles. In fact, we discussed scenarios where the impedance profiles are relatively close to one another, but the envelope responses show significant differences between the corresponding cases. Our results also show some small discrepancies between the two methods used to compute the impedance profile (the one based on the envelope responses for sequences of sinusoidal inputs at different frequencies and the one based on the use of a ZAP inputs). These differences are not likely to be the results of the presence of slow processes, since the system is two-dimensional, but the result of the ZAP output capturing some transient effects. Finally, while the impedance profile captures the non-uniform amplitude response mentioned above by having a second peak lower than the resonant one (Fig. 10-b2), the shape of the voltage response cannot be inferred from the impedance graph since the second peak may be the result of deformations in the output cycle. Note that the impedance profile captures the output amplitude versus the output frequency, not versus the input frequency. This consideration is irrelevant for linear models since the input and output frequencies coincide, but it is important for the interpretation of the preferred frequency responses of nonlinear models.

Additional research is needed to test the results and ideas generated by our work in more complex and realistic EC models and to experimentally test the predictions of our results and the results from these subsequent studies. They should use more realistic inputs and dimensional equations. A natural extension of our work should include the use of potential oscillatory inputs instead of current oscillatory inputs. Dynamically, the main difference between these two protocols is that the input affects both equations instead of affecting only one. This implies that extended phase-plane diagram includes to moving nullclines instead of only one. Further research is also needed to determine the mechanisms responsible for the response patterns to oscillatory inputs generated by more complex models. Particularly the emergence of antiresonance known to be present in higher-dimensional models in EC and other biological systems [4, 8, 15, 20]. The methods we developed in this paper could be adapted to address the mechanisms of generation of these more complex patterns.

Acknowledgments

This work was partially supported by the NSF grant DMS-1313861 (HGR).

References

[1] M. T. M. Koper. Nonlinear phenomena in electrochemical systems. *J. Chem. Soc. Faraday Trans.*, 94:1369–1378, 1998.

[2] B. Hutcheon and Y. Yarom. Resonance, oscillations and the intrinsic frequency preferences in neurons. *Trends Neurosci.*, 23:216–222, 2000.

[3] H. G. Rotstein. Preferred frequency responses to oscillatory inputs in an electrochemical cell model: Linear amplitude and phase resonance. *Phys. Rev. E*, 88:062913, 2013.

[4] M. J. E. Richardson, N. Brunel, and V. Hakim. From subthreshold to firing-rate resonance. *J. Neurophysiol.*, 89:2538–2554, 2003.

[5] H. G. Rotstein and F. Nadim. Frequency preference in two-dimensional neural models: a linear analysis of the interaction between resonant and amplifying currents. *J. Comp. Neurosci.*, 37:9–28, 2014.

[6] H. G. Rotstein. Frequency preference response to oscillatory inputs in two-dimensional neural models: a geometric approach to subthreshold amplitude and phase resonance. *J. Math. Neurosci.*, 4:11, 2014.

[7] H. G. Rotstein. Subthreshold amplitude and phase resonance in models of quadratic type: nonlinear effects generated by the interplay of resonant and amplifying currents. *J. Comp. Neurosci.*, 38:325–354, 2015.

[8] H. G. Rotstein. Resonance modulation, annihilation and generation of antiresonance and antiphasonance in 3d neuronal systems: interplay of resonant and amplifying currents with slow dynamics. *J. Comp. Neurosci.*, 43:35–63, 2017.

[9] S. H. Strogatz. *Nonlinear Dynamics and Chaos*. Addison Wesley, Reading MA, 1994.

[10] M. T. M. Koper. Stability study and characterization of electrochemical oscillators by impedance spectroscopy. *J. Electroanal. Chem.*, 409:175–182, 1996.

[11] I. Kiss, V. Gáspár, and L. Nyikos. Stability analysis of the oscillatory electrodissolution of copper with impedance spectroscopy. *J. Phys. Chem. A*, 102:909–914, 1998.

[12] M. Naito, N. Tanaka, and H. Okamoto. General relationship between complex impedance and linear stability in electrochemical systems. *J. Chem. Phys*, 111:9908–9917, 1999.

[13] A. Karantonis, E. Bourbos, and D. Koutsaftis. Electrochemical resonance: frequency response analysis of the electrodissolution of copper in trifluoroacetic acid close to dynamic instabilities. *Chem. Phys. Lett.*, 490:69–71, 2010.

[14] A. Karantonis and D. Karaoulanis. Conditions of electrochemical resonance under potentiostatic control. *Electrochimica Acta*, 56:4119–4125, 2011.

[15] A. Karantonis and D. Karaoulanis. Electrical resonance and antiresonance of the electrochemical interface under potentiostatic control: Theoretical considerations. *Electrochimica Acta*, 78:244–250, 2012.

[16] A. Karantonis, E. Bourbos, and D. Karaoulanis. Experiments on electrical resonance and antiresonance of the electrochemical interface under potentiostatic control. *Electrochimica Acta*, 87:912–917, 2013.

[17] A. Karantonis, M. Pagitsas, and D. Sazou. Dynamical response of the sinusoidally perturbed electrodissolution/ passivation of iron in sulfuric acid solutions : Entrainment, spike generation, and quasiperiodicity. *Chaos*, 3:243–256, 1993.

[18] D. Karanoulanis, P. Chhryssafidis, and A. Karantonis. Electrochemical resonance under harmonic current perturbations and chaotic potential perturbations. *J Solid State Electrochem*, 19:3277–3286, 2015.

[19] H. G. Rotstein. Subthreshold resonance and phasonance in single cells: 2D models. *In: Jaeger D., Jung R. (Ed.) Encyclopedia of Computational Neuroscience: SpringerReference (www.springerreference.com). Springer-Verlag, New York*, 2018.

[20] H. G. Rotstein. Subthreshold antiresonance and antiphasonance in single cells: 3D models. *In: Jaeger D., Jung R. (Ed.) Encyclopedia of Computational Neuroscience: SpringerReference (www.springerreference.com). Springer-Verlag, New York*, 2018.

[21] I. Z. Kiss, W. Wang, and J. L. Hudson. Populations of coupled electrochemical oscillators. *Chaos*, 12:252–263, 2002.

[22] P. Kaira, P. S. Bodega, C. Punckt, H. H. Rotermund, and D. Drefting. Pattern formation in 4:1 resonance of the periodically forced CO oxidation of Pt(110). *Phys. Rev. E*, 77:0461060, 2008.

[23] A. Karantonis and S. Nakabayashi. Phase flow deformations and coupled electrochemical oscillators. *Chem. Phys. Lett.*, 347:133–137, 2001.

[24] M. T. M. Koper and J. H. Sluyters. A mathematical model for current oscillations at the active-passive transition in metal electrodissolution. *J Electroanal Chem*, 347:31–48, 1993.

[25] P. Parmananda, J. Gerardo, M. Escalera Santos, and K. Showalter. Stochastic resonance of electrochemical aperiodic spike trains. *Phys. Rev. E*, 71:031110, 2005.

[26] R. FitzHugh. Impulses and physiological states in models of nerve membrane. *Biophysical J.*, 1:445–466, 1961.

[27] J. S. Nagumo, S. Arimoto, and S. Yoshizawa. An active pulse transmission line simulating nerve axon. *Proc. IRE*, 50:2061–2070, 1962.

[28] E. Puil, B. Gimbarzevsky, and R. M. Miura. Quantification of membrane properties of trigeminal root ganglions in guinea pigs. *J. Neurophysiol.*, 55:995–1016, 1986.

[29] H. G. Rotstein. Spiking resonances in models with the same slow resonant and fast amplifying currents but different subthreshold dynamic properties. *J. Comp. Neurosci.*, 43:243–271, 2017.

[30] M. Espanõl and H. G. Rotstein. Complex mixed-mode oscillatory patterns in a periodically forced excitable chemical reaction model. *Chaos*, 25:064601, 2015.

[31] A. Birzu and K. Krischer. Resonance tongues in a system of globally coupled oscillators with time-periodic coupling strength. *Chaos*, 20:043114, 2010.

[32] E. Izhikevich. *Dynamical Systems in Neuroscience: The geometry of excitability and bursting.* MIT Press (Cambridge, Massachusetts), 2006.

[33] H. G. Rotstein, N. Kopell, A. Zhabotinsky, and I. R. Epstein. A canard mechanism for localization in systems of globally coupled oscillators. *SIAM J. Appl. Math.*, 63:1998–2019, 2003.